Cross-Linking

International Edition: DOI: 10.1002/anie.201912902
German Edition: DOI: 10.1002/ange.201912902

Covalent Adaptable Networks with Tunable Exchange Rates Based on Reversible Thiol–yne Cross-Linking

Niels Van Herck, Diederick Maes, Kamil Unal, Marc Guerre, Johan M. Winne, and Filip E. Du Prez**

Abstract: *The design of covalent adaptable networks (CANs) relies on the ability to trigger the rearrangement of bonds within a polymer network. Simple activated alkynes are now used as versatile reversible cross-linkers for thiols. The click-like thiol–yne cross-linking reaction readily enables network synthesis from polythiols through a double Michael addition with a reversible and tunable second addition step. The resulting thioacetal cross-linking moieties are robust but dynamic linkages. A series of different activated alkynes have been synthesized and systematically probed for their ability to produce dynamic thioacetal linkages, both in kinetic studies of small molecule models, as well as in stress relaxation and creep measurements on thiol–yne-based CANs. The results are further rationalized by DFT calculations, showing that the bond exchange rates can be significantly influenced by the choice of the activated alkyne cross-linker.*

Introduction

Covalent adaptable networks (CANs) are polymer materials that combine the strength of covalently cross-linked materials, such as high chemical resistance and dimensional stability, with the reprocessability of thermoplastic polymers.[1–4] These responsive polymer networks have the ability to reversibly rearrange their network topology through the action of dynamic exchanges. Upon application of an external stimulus (such as heat, light), the dynamic chemistry is activated to allow bond exchanges on a molecular level, which enables network plasticity and allows reshaping, reprocessing, stress relaxation, self-healing, and imprinting.

[*] N. Van Herck, D. Maes, K. Unal, Dr. M. Guerre, Prof. Dr. F. E. Du Prez
Polymer Chemistry Research Group, Center of Macromolecular Chemistry (CMaC), Department of Organic and Macromolecular Chemistry, Faculty of Sciences, Ghent University
Krijgslaan 281 (S4-bis), 9000 Ghent (Belgium)
E-mail: Filip.DuPrez@UGent.be

K. Unal, Prof. Dr. J. M. Winne
Laboratory for Organic Synthesis, Department of Organic and Macromolecular Chemistry, Faculty of Sciences, Ghent University
Krijgslaan 281 (S4), 9000 Ghent (Belgium)
E-mail: Johan.Winne@UGent.be

Dr. M. Guerre
Laboratoire des IMRCP, Université de Toulouse, CNRS UMR 5623, Université Paul Sabatier
118 route de Narbonne, 31062 Toulouse Cedex 9 (France)

Supporting information and the ORCID identification number(s) for the author(s) of this article can be found under: https://doi.org/10.1002/anie.201912902.

An important characteristic of CANs is the underlying bond exchange mechanism as it ultimately determines the mechanical properties of a CAN during the applied stimulus.[3] Reversible polymer networks or so-called dissociative CANs imply that a bond-breaking event happens prior to the formation of a new bond (that is, an elimination–addition mechanism), whereas bond exchange in permanent dynamic networks, also called vitrimers or associative CANs, is achieved through a bond-forming/bond-breaking sequence (an addition–elimination reaction).[1,5] As a result, dissociative CANs can show a temporary decrease in network connectivity during the stimulus application, which may result in a sudden decrease of viscosity, while associative CANs or vitrimers, preserve their network integrity in all conditions and do not undergo a gel-to-sol transition.[6] In this regard, many different chemistries have now been applied or purposely developed for CANs. For example, typical dissociative reversible systems are based on furan–maleimide chemistry,[7] alkoxyamine chemistry,[8] triazolinedione–indole chemistry,[9–11] phthalate monoester transesterification,[12] and so on, while typical associative reversible systems are based on transesterification,[13] vinylogous urethane transamidation,[14–17] transalkylation,[18,19] allyl sulfide exchange,[20] or boroxine exchange.[21]

As part of our group's continuing interest towards CANs and the exploration and development of new reversible chemistry platforms for their design, we were inspired by the base-catalyzed dynamic equilibria of thiols and activated alkenes. Although thiol–ene reactions are long-known in polymer chemistry as click-like bond forming reactions, their reversible nature has only recently been explored in polymer chemistry by Konkolewicz and co-workers (Scheme 1 a).[22] Further inspired by recent work by Kalow and co-workers using thioacetals as versatile dynamic cross-links (Scheme 1 b),[23] we became intrigued by the possibility of using simple activated alkynes, such as alkynones, directly as cross-linkers for thiol-based monomers and polymers, in a straightforward way resulting in possibly highly dynamic thioacetal linkages, starting from very simple precursors (Scheme 1 c).

In fact, the base-promoted dynamics of alkynone-derived thioacetals (see Scheme 1 c) was investigated on small molecule level by Anslyn and co-workers in 2012.[24] In this encouraging prior study, it was shown that the dynamic thiol exchange of thioacetals via retro-Michael reactions (vinylogous thioesters) was possible, and can thus likely be tuned for interesting applications in the context of dynamic combinatorial libraries.[25] Recently, there has been a surge in reports on CANs that rely on dynamic thiol exchange via reversible thiol-Michael chemistry,[22,26–28] transthioesterification[29] and reversible exchange at

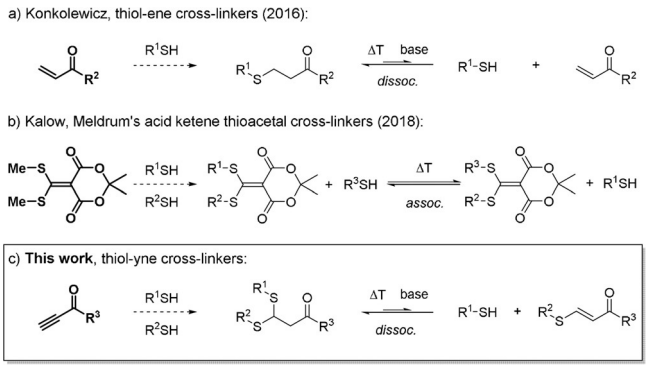

Scheme 1. Overview of dynamic thiol exchange chemistries for polymer networks: a) Reversible thiol–ene Michael reaction of thiols and activated alkenes, b) ketene thioacetal exchanges through reversible Michael additions to a Meldrum's acid derivative, c) investigated reversible thiol–yne Michael reactions of thiols and activated alkynes.

a Meldrum's acid alkylidene.[23] As the currently available thiol-based dynamic chemistries either require exotic reagents, free thiols that are prone to side reactions (such as oxidation), long relaxation times or aqueous basic conditions to allow exchange, we envisaged that the thiol–yne-derived dynamic thioacetal links could thus provide a quite valuable and complementary addition to the growing toolbox of dynamic thiol-click chemistries.[30–32] The very specific two-step mechanism of the double Michael addition on an ynone moiety studied in this work offers two important advantages over existing thiol-based dynamic cross-linking chemistries. From a fundamental or pure polymer chemistry point of view, it can be expected that both the kinetics and the thermodynamics of bonding and debonding can be controlled (tunability) through introduction of substituents on key position of the activated yne, offering options to control the rate of exchange and the degree of connectivity, thereby bridging the standard situation of permanent versus non-permanent dynamic networks. This chemistry thus presents a good testing ground for new ideas, with many handles to control reactivity. Furthermore, from a very practical or applied polymer chemistry point of view, monofunctional ynone- or ynoate-type compounds can be directly used as bivalent cross-linkers for thiol moieties, making their practical application and synthesis cost less challenging.

In this work, we thus aimed for the exploration of dynamic thiol–yne cross-linking as a new platform for the dynamic exchange of thioacetal linkages. The most desirable reactivity profiles in terms of CANs were first explored using kinetic studies on model compounds, followed by stress relaxation measurements on material level. It was found that the exchange rate could be controlled through the judicious choice of the alkynone (or activated alkyne) cross-linker. The observed influence of the alkynone structure on the exchange rate was further evaluated by density functional theory (DFT) calculations, which confirmed and could rationalize the experimental observations. The obtained polymer networks were subjected to extensive mechanical, thermal, stress relaxation and reprocessing tests to demonstrate the desired dynamic behavior.

Results and Discussion

The key functional monomers and cross-linkers used in this work are activated alkyne moieties (**X**, Scheme 2) like conjugated alkynones, that can serve as double Michael acceptors. Such moieties are readily available or can be easily prepared from simple precursors. A base-catalyzed click-reaction with two thiols can then result in a thioacetal derivative of **X** (**TA-X**,

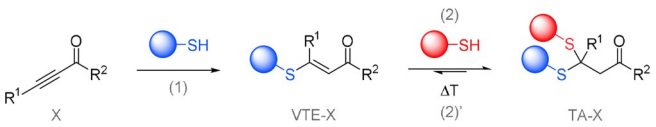

Scheme 2. Synthesis of a thioacetal adduct (**TA-X**) via the base-catalyzed double thiol-Michael addition on alkynone precursors (**X**). (**VTE-X**) represents the β-sulfido-α,β-unsaturated carbonyl intermediate. Reaction (2′) corresponds to the dynamic thiol exchange occurring at high temperature.

Scheme 2). The basic catalyst promotes deprotonation of the thiol to its more nucleophilic thiolate form, which performs the first Michael addition (Reaction (1), Scheme 2) on the electron-deficient triple bond of the alkynone. This can yield both isomers (*E*/*Z*) of the β-sulfido-α,β-unsaturated carbonyl or vinylogous thioester derivative of the alkynone **X** (**VTE-X**).[24,33] Subsequently, this initial Michael adduct can act again as a Michael acceptor to allow a second thiol addition (Reaction (2), Scheme 2). In previous studies, this second addition has been shown to be up to 1000 times slower than the first addition.[34] The resulting final product, the thioacetal derivative **TA-X**, can nevertheless be obtained in very high overall yields (Table 1), depending on the used catalyst.[31,34–36] This double-addition reaction pathway was first verified and monitored by ^{1}H NMR spectroscopy for the reaction between a simple alkynone, but-3-yn-2-one (**X** = **1**, Table 1), and 2 equiv of butane-1-thiol (Supporting Information, Figure S1). Using only 1 mol% of 1,5,7-triazabicyclo[4,4,0]dec-5-ene (TBD) as a catalyst, the desired thioacetal adduct (**TA-1**) could be synthesized within 10 minutes at room temperature in chloroform with 95% yield. In these studies, TBD was chosen as a non-nucleophilic, strong, non-volatile and lipophilic base that is compatible with polymer formulations and their envisaged thermal reprocessing, and also immediately gave very good results on small molecule level.[35]

Even though the forward reactions to yield the thioacetal adduct are spontaneous and thermodynamically favored, Anslyn reported that dynamic thiol exchange can happen upon the addition of alternative thiols and triethylamine in solution via the suspected retro-Michael reaction (2′) in Scheme 2.[24] As our objective was to explore the utility of this reversible reaction in the context of CANs with dynamic thiol–yne derived thioacetal linkages, we first synthesized a series of small molecule **TA-X** compounds following the synthetic procedure depicted above (1 mol% TBD in chloroform). With these thioacetals in hand, the dynamic thiol exchange was evaluated at elevated temperature by means of kinetic studies through the monitoring of reaction progress via ^{1}H NMR spectroscopy.

Table 1: Overview of investigated alkynones (**X**) with their corresponding experimental data on model compound and material level.

Entry	X	VTE-X[a] Yield [%]	TA-X[b] Yield [%]	Model study E_a [kJ mol^{-1}]	Rheology E_a [kJ mol^{-1}]
	**1**	99	95	76.8 ± 4.4	137.4 ± 1.8
	**2**	99	94	/[d]	197.8 ± 2.5
	**3**	99	81	71.0 ± 4.9	128.4 ± 0.3
	**4**	63[c]	92	76.2 ± 2.1	134.1 ± 0.6
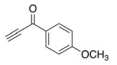	**5**	99	81	74.4 ± 3.8	178.6 ± 1.1
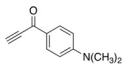	**6**	99	93	75.4 ± 2.6	186.5 ± 6.8
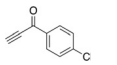	**7**	92	88	66.2 ± 14.9	133.5 ± 1.0
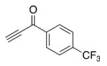	**8**	83[c]	95	66.2 ± 1.3	124.3 ± 1.1
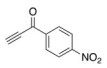	**9**	35[c]	97	75.1[e]	128.0 ± 1.1
	**10**	99	25	–	–
	**11**	93	0	–	–
	**12**	99	34	–	–
	**13**	99	27	–	–
	**14**	99	6	–	–
	**15**	99	85	/[d]	–

[a] Yield after addition of 1 equiv thiol. [b] Yield after addition of 2 equiv thiol. [c] Yield of isolated **VTE-X** was lower than expected as a result of overreaction, generating the double thiol-Michael product **TA-X**. [d] Activation energy E_a could not be determined as no exchange was observed in the investigated temperature range. [e] E_a could not be determined in a reliable way since exchange was too fast to collect kinetic data above 40 °C.

Synthesis of Model Compounds

To explore the scope and possible limitations of the thiol–yne dynamic chemistry platform for CANs, a wide series of alkynone-type double Michael acceptors (**X**) was selected or prepared (Table 1) and then evaluated for their click-like ability to reliably form thioacetal cross-linkages (**TA-X**) (see Scheme 2). Only limited examples of double Michael additions to alkynones can be found in the literature, and the success of these reactions can be expected to be dependent on steric and electronic factors, where the second Michael reaction could theoretically favor either the **VTE-X** or the **TA-X** side. A high yield for this step is certainly possible, but is thus not guaranteed (see for example the entry where **X** = **12**). The substituents directly bound to the alkyne function (Scheme 2, R^1), as well as the substituents directly bound to the carbonyl function (R^2) were varied with the intent to probe both steric and electronic effects on the dynamic exchange. In this series of alkynones, but-3-yn-2-one (**X** = **1**) was arbitrarily selected as the benchmark to which all other alkynones will be compared. Alkynones **2**, **13**–**15** were chosen to evaluate the effect of replacing the ketone functionality with an ester, amide, sulfonamide, or sulfone, respectively, as these are also common moieties in polymer chemistry. Alkynones **3**–**9** represent derivatives of 1-phenyl-prop-2-yn-1-one, which allowed the exploration of the hypothetical control on the exchange through introduction of electronically (de)activating *para*-substituents. Alkynones **10**–**12** were chosen to evaluate the effect of substituents directly bound to the alkyne function. All alkynones were synthesized according to known literature procedures[37–42] (see the Supporting Information), except for alkynones **1**, **2** and **12**, which are commercially available.

In a next step, the dynamics of the most readily obtained model compounds (**TA-X**) were evaluated by kinetic exchange studies. Table 1 shows overall very good yields for the first thiol-Michael addition to yield **VTE-X** compounds. For **VTE-4**, **VTE-8**, and **VTE-9**, the yield of isolated product was lower than expected only because of the very swift second Michael addition reaction, directly generating the double thiol-Michael product **TA-X**. However, the activated alkyne substrates **10**–**14** showed an incomplete second addition and were not further considered during the kinetic model studies or network synthesis, as they cannot serve as a thiol–yne-type cross-linker. This lower efficiency of the second thiol Michael reaction can be related to electronic and steric considerations. Thus, only the alkynones that gave highly efficient double thiol-Michael additions with butane-1-thiol were further considered for our current investigations (see the Supporting Information).

Kinetic Model Studies

To evaluate the dynamic behavior of the synthesized thioacetal adducts (**TA-X**), stock solutions containing **TA-X**, 1 mol% TBD and an internal standard in deuterated benzene were prepared, followed by the addition of a fivefold excess of benzyl mercaptan as a competitive thiol to approach pseudo first-order conditions for the initial exchange rates (see the Supporting Information for experimental details). During the exchange reaction, the butanethiol groups of the respective model compound were found to be gradually replaced by benzyl mercaptan groups, leading to the formation of a mixture of three different thioacetals: **TA-X$_{AA}$**, **TA-X$_{AB}$**, **TA-X$_{BB}$**, where AA, AB, and BB describe the alkyl groups present in the thioacetal adduct: butane/butane, butane/benzyl, and benzyl/benzyl, respectively (Figure 1a for **TA-1**). The exchange reaction was monitored by following the characteristic ^{1}H NMR signal of the original thioacetal motif (**TA-X$_{AA}$**, triplet at 4.35–4.50 ppm), which decreased in intensity, while the new thioacetal signals of the exchanged products (**TA-X$_{AB}$**, **TA-X$_{BB}$**) emerged upfield (Figure 1b). The remaining molar fraction of **TA-X$_{AA}$** was followed over time to determine the rate constant *k*. This was repeated at different temperatures comprised between 40 and 70 °C, which allowed creating an Arrhenius plot from which the activation energy E_a could be deduced as the slope of the linear fit (see the Supporting Information).

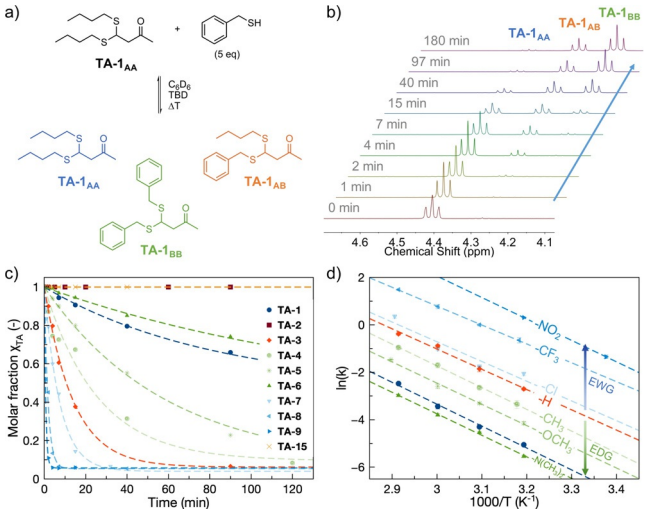

Figure 1. a) Dynamic thiol exchange of **TA-1** at elevated temperature with benzyl mercaptan, leading to three different exchange products: **TA-1$_{AA}$**, **TA-1$_{AB}$**, **TA-1$_{BB}$**. b) Evolution of characteristic ^{1}H NMR signals of the thioacetal motifs over time. c) Overlay of remaining molar fraction of **TA-X** as a function of time during the exchange experiment at 40 °C. Dashed lines represent a fit with exponential decay. d) Arrhenius plots of the reversible model compounds. Dashed lines represent a linear fit (the same color legend as in (c) applies). Chemical formulas represent the *para*-substituents of 1-phenylprop-2-yn-1-one-derived compounds (**TA-X**, with **X** = **3**–**9**).

Figure 1c shows an overlay of the remaining molar fractions of **TA-X** as a function of time during the exchange experiments at 40 °C. Interestingly, the exchange kinetics were significantly influenced by the used model compound. Compared to the benchmark **TA-1**, some model compounds showed a remarkably faster dynamic thiol exchange, whereas others showed slower or even no exchange. From the Arrhenius plots in Figure 1d, similar activation energies E_a within the range of 66–77 kJ mol^{-1} were obtained for all reactions (Table 1). This could be expected since the exchange mechanism should be unchanged regardless of the used model compound. Nevertheless, a small trend could be observed in the data for the series of phenylpropynone-based model compounds (**TA-X**, with **X** = **3**–**9**). When the activation energy of **TA-3** (no substituent on phenyl group) was taken as a reference (E_a = 71 kJ mol^{-1}), the introduction of electron donating *para*-substituents (**X** = **4**–**6**) added a penalty of 3–5 kJ mol^{-1} to the energy barrier, whereas electron withdrawing *para*-substituents (**X** = **7**–**9**) reduced this barrier by 5 kJ mol^{-1}. As can be expected, the anionic transition state, that is, when a thiolate anion is attacking the Michael acceptor, will be selectively stabilized over the neutral ground states, by the presence of electron withdrawing substituents on the aromatic ring conjugated to the receiving carbonyl function. However, considering that the small difference in E_a is within experimental error for some model compounds, this interpretation of the temperature dependencies of the exchange rates remains speculative.

Nevertheless, the same trend in electronic activation is found to have a major effect on the actual exchange rates, spanning several orders of magnitude, as can be clearly seen in the Arrhenius plot (Figure 1d). It is very clear from these data that electron-withdrawing substituents accelerate the exchange significantly, whereas electron donating substituents showed the reverse effect (that is, lower rate constants). The fastest exchange was observed for **TA-9**, where the introduction of a nitro group (−NO_2) allowed complete exchange within 2 minutes at 40 °C, even causing problematic sampling at higher temperatures. Conversely, the slowest exchange was observed for the analogous compound **TA-6**, where the only difference is the introduction of an electron-donating dimethylamino group (−$N(CH_3)_2$), showing only 50 % conversion after 4 hours at 40 °C. The influence of *para*-substituents on the exchange rate was also confirmed through Hammett analysis (Supporting Information, Figure S2), which showed a strong positive linear correlation indicating an exchange mechanism via anionic intermediates.[43,44]

Another interesting observation was that model compounds **TA-2** and **TA-15** did not show exchange at the investigated temperature and timescale. Hence, they could be considered as practically irreversible, owing to the presence of the intrinsically less electron-withdrawing ester or sulfone functional group. As intermediate conclusion, these results already indicated that the choice of the alkynone precursor is quite important with respect to the reversible nature of the thioacetal motif. Moreover, these experiments showed that the exchange rate could be significantly manipulated by means of the electronic substituents on the alkynone precursor.

For the design of CANs, the nature of the bond exchange mechanism is a key parameter since it dictates the viscoelastic profile of the resulting materials. The mechanism will also rely on the conditions and stoichiometry, and the reaction conditions for the model experiments described above may thus be a poor substitute for those found in thiol–yne-based polymer networks, where there may not be large amounts of free thiols present. Thus, to probe the thioacetal exchange in a more realistic setting, we also investigated whether the bond exchange can happen in the absence of free thiols. Therefore, two different thioacetal adducts were synthesized by reacting alkynone **1** with either butane-1-thiol (**TA-1$_{AA}$**) or benzyl mercaptan (**TA-1$_{BB}$**). In a next step, these model compounds were mixed in a 1:1 stoichiometric ratio in deuterated benzene in the presence of TBD and heated to 70 °C. ^{1}H NMR analysis revealed the gradual appearance of the mixed thioacetal moiety (that is, **TA-1$_{AB}$**) over time, which indicates that no free thiols are required to allow exchange (Supporting Information, Figure S3). However, the exchange was found to proceed more slowly compared to the model experiments where an excess of free thiols was present. This result indicates that, while exchange rates are already fast at room temperature in our small molecule models, the situation inside a polymer network may be quite different as the exchange will also rely on statistics and diffusion limitations, therefore not directly reflecting the intrinsic chemical reaction rate.

DFT Calculations

Intrigued by the remarkable effect of the used alkynone precursor on the exchange kinetics, density functional theory calculations were also performed to confirm these observations.

The Gaussian16 package was used with the M06-2X/6-311+G(d,p) level of theory, which has been shown successful to describe the thermodynamics of the thiol-Michael addition (see the Supporting Information for computational details).[45] Using this theoretical method, the calculated Gibbs free energy profile of the double thiol-Michael addition on the alkynone compound (**X**) could be modeled (Supporting Information, Figures S24–S37 and Table S2). The most crucial parameter coming out of this calculational approach is the relative Gibbs free energy of the transition state of the rate limiting step of the pathway ($\Delta G^{\circ,\ddagger}$), referenced to the energetic ground state of the reactants and products.

In the graphical summary of these calculations (Figure 2), all of the thiol-Michael additions to the **VTE-X** intermediates are exergonic, with a thermodynamic driving force between only 15–20 kJ mol^{-1}. This readily indicates and confirms the reversible nature of this second bond formation step. The thermodynamic profiling of the individual reaction pathways is more challenging and subject to interpretation, but the relative Gibbs free-energy difference for the modeled transition states, with reference to the ground states of the thioacetal adducts, indeed closely matches the trends observed in our kinetic experiments. Indeed, thiol exchange could only occur when the energetic barrier of $\Delta G^{\circ,\ddagger}$ is overcome to allow dissociation of the thioacetal (**TA-X**) into the vinylogous thioester (**VTE-X**) and thiolate anion. Therefore, this parameter is closely related to the activation energy E_a as experimentally determined earlier during kinetic model studies.

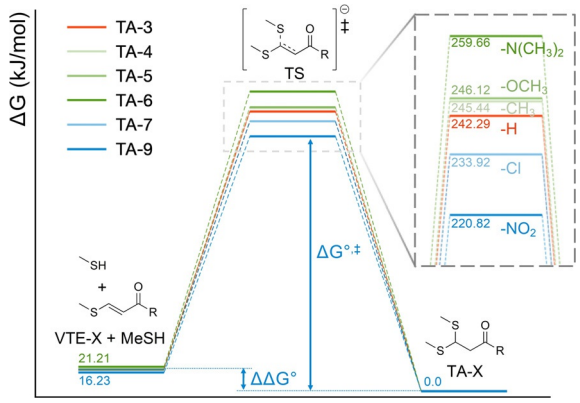

Figure 2. Calculated free-energy diagram for the second thiol-Michael addition of methanethiol to **VTE-X** (with **X**=**3**–**9**) with the formation of the **TA-X** product via the corresponding transition state (TS). The zoomed section shows the difference in $\Delta G^{\circ,\ddagger}$.

Interestingly, these calculations also provided a means to rationalize the incomplete formation of the desired thioacetal adducts from alkynones **10** and **13**. In contrast to all other modeled **VTE-X**, the DFT-derived reaction Gibbs free energy for thiol addition to **VTE-10** was found to favor the de-bonded state (Supporting Information, Table S2). The reaction Gibbs free energy for **10** is calculated as slightly endergonic ($\Delta\Delta G^{\circ}_{10}$ = 0.61 kJ mol^{-1}; Supporting Information, Figure S33), indeed predicting an equilibrium mixture of **VTE-10** and **TA-10**, as is experimentally observed. The same reasoning could not be applied to explain the incomplete formation of **TA-13**, as the reaction itself was found to be clearly exergonic by our calculation. However, the low yield for **TA-13** could be attributed to the higher forward energetic barrier ($\Delta G^{\circ,\ddagger}$), which may substantially slow down the second Michael reaction. The latter was also observed experimentally, as only 27% conversion of **TA-13** was reached after 1 week at room temperature.

Our DFT model was unable to provide a rationalization for the distinct difference in reactivity observed for the seemingly non-reversible adducts **TA-2** and **TA-15**, as comparable energy profiles were in fact obtained here (see the Supporting Information). Thus, more advanced models may be required here.

Synthesis of CANs

Based on the outcome of the small-molecule model study, the most interesting alkynones were selected for further investigation on a material's level. Alkynones **1** and **3**–**9** were expected to result in reversible cross-links in a dynamic polymer network, whereas alkynone **2** was assumed to give an irreversible material. Since alkynones have a functionality (f) of 2, the combination of an activated alkyne with any multifunctional thiol with $f \geq 3$ should directly result in a cross-linked polymer network. Originally, reaction of the alkynones with the commercially available pentaerythritol tetrakis(3-mercaptopropionate) was considered for the synthesis of polymer networks. However, this tetrafunctional thiol contains ester bonds, which are known to exchange via transesterification reactions in the presence of TBD.[46] Therefore, this thiol was not suited for unambiguous design of dynamic materials that are solely relying on dynamic thiol exchange. Hence, an aliphatic trifunctional thiol (trithiol)[47] was synthesized and used as a reference building block to produce dynamic polymer materials.

Thiol–yne polymer networks were prepared through reaction of the alkynone of interest with trithiol in the presence of TBD (see Scheme 3 and the Supporting Information for experimental details). First, a vinylogous thioester prepolymer (**VTEp-X**) was prepared using 1 equiv of trithiol with 3 equivalents of alkynone. In a second step, another equivalent of trithiol was added to the prepolymer to produce and fully cure the polymer network (**CAN-X**). As a result of this two-step

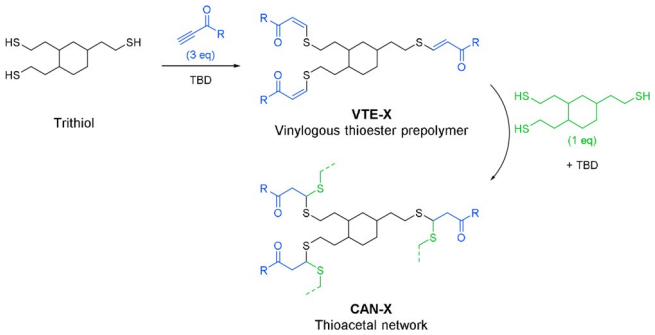

Scheme 3. Network synthesis via the reaction of trithiol (1 equiv) with alkynone (3 equiv) in the presence of TBD to yield the vinylogous thioester prepolymer (**VTEp-X**), followed by addition of trithiol (1 equiv) to produce a thioacetal cross-linked network (**CAN-X**).

method, also the relatively high exotherm associated with the double thiol-Michael addition could be better controlled, resulting in well-defined and reproducible network formation at completely stoichiometric conditions, theoretically containing no free thiols. The prepared networks were transparent and displayed a slight coloration depending on the used alkynone (Supporting Information, Figure S4).

High resolution magic angle spinning (HRMAS) ^{1}H NMR was used to confirm the presence of the thioacetal motif in the prepared polymer networks (Supporting Information, Figure S5). Deuterated chloroform was selected as a non-reactive solvent providing very good swelling. Using this technique, a conversion of 85–90 % could be estimated (residual VTE-signals integrating for ca. 10 %), which is presumably caused by diffusion limitations in these highly cross-linked networks. Thus, the degree of polymerization should be well above the theoretical gel point (71 %) according to the Flory–Stockmayer theory for a trifunctional (A_3) and difunctional monomer (B_2).[48,49] To further confirm network formation, swelling experiments were performed in tetrahydrofuran (THF) at room temperature to determine the soluble fraction for **CAN-1** and **CAN-3** as representative networks (Supporting Information, Table S1). Those networks showed a swelling ratio between 120–300 % and a soluble fraction below 3 %.

Thermal analysis of CANs

Thermogravimetric analysis (TGA) of the prepared polymer networks demonstrated a single decomposition step with a maximum degradation rate at ±330 °C for most of the networks (Figure 3a). **CAN-4** and **CAN-6** also showed an earlier decomposition step with an onset (5 % weight loss) degradation temperature of $T_{d5\%} = 176$ and 149 °C, respectively.

Differential scanning calorimetry (DSC) revealed the presence of a glass transition temperature (T_g) that varied within the range of −16 to 52 °C depending on the used alkynone precursor (Figure 3b). Since all of the networks were prepared in the same way, this variable rigidity was attributed to the presence of freely rotating groups and conjugated π systems in the alkynone compound. An increased T_g was observed when a larger conjugated system was present in the matrix (**CAN-3** vs. **CAN-9**). Interestingly, the simple presence of a (freely rotating) methoxy group in **CAN-5** resulted in a very pronounced decrease of T_g. Besides the glass transition, an endotherm starting at 120 °C was observed, which was attributed to the activation of the retro-Michael reaction at this temperature.

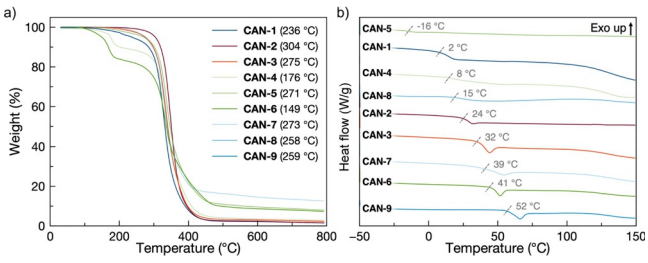

Figure 3. Thermal analysis of CANs. a) Overlay of TGA thermograms. Values in brackets are the onset degradation temperatures at 5 % weight loss ($T_{g5\%}$). b) Overlay of DSC thermograms (2nd heating). The onset T_g is displayed above each trace.

Rheological analysis of CANs

To examine the viscoelastic properties of the dynamic networks, stress relaxation experiments were performed. During these measurements, a constant strain of 1 % was applied and the relaxation modulus was followed as a function of time at different temperatures. Typical stress relaxation curves are presented in Figure 4a for **CAN-1** and in the Supporting Information, Figures S6–S13 for all other CANs. As a result of dynamic bond rearrangement at high temperatures, full stress relaxation of the networks could be obtained. Next, relaxation times (τ) were determined at 37 % ($1/e$) of the normalized relaxation modulus (G/G_0) according to the Maxwell model for viscoelastic fluids and plotted in an Arrhenius plot to obtain the corresponding viscous flow activation energy E_a of 137 kJ mol^{-1} for **CAN-1** (Figure 4b).[50]

The relaxation measurements were performed below 150 °C for most networks (except **CAN-1** and **CAN-2**) to prevent degradation of the TBD catalyst.[51] In the case of **CAN-1**, an upper temperature of 170 °C was used to increase the number of data points in the Arrhenius plot. For **CAN-2**, which was actually prepared as a reference material with the expectation of being an irreversible network, a slight stress relaxation was observed at 150 °C (Supporting Information, Figure S6), which encouraged us to explore the limits of this material. Therefore, relaxation measurements were performed until an upper

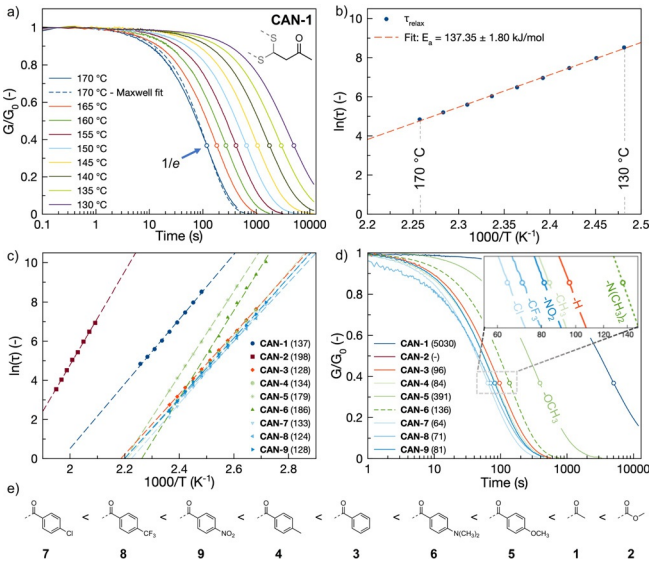

Figure 4. a) Stress relaxation experiment of **CAN-1** between 130 and 170 °C. Relaxation times (τ) were determined at $G/G_0 = 1/e$. b) Arrhenius plot of the obtained relaxation times with linear fit according to Arrhenius equation and the corresponding viscous flow activation energy (E_a). c) Overview of Arrhenius plots with linear fits for all networks. Values in brackets represent the activation energy in kJ mol^{-1}. d) Overview of stress relaxation curves at 130 °C for all networks. Values in brackets represent the relaxation time (at $1/e$) in seconds at 130 °C. For **CAN-6** a Maxwell fit (dashed line) was created for clear comparison. e) Ranking of CANs with regard to relaxation time at 130 °C.

temperature as high as 240 °C to probe the possible bond exchange via **VTE-2**-type moieties (see above). Indeed, full stress relaxation could be observed if enough energy was added to the system (Supporting Information, Figure S6).

An overview of all Arrhenius plots is presented in Figure 4c. With the exception of **CAN-6**, all networks exhibited a linear correlation of $\ln(\tau)$ with $1000/T$ in the observed temperature window, indicating Arrhenius flow characteristics. The unusual stress relaxation curves of **CAN-6** (Supporting Information, Figure S10) were attributed to the absence of a rubbery plateau within this temperature range, which was confirmed by temperature sweep measurements (Supporting Information, Figure S14). The Arrhenius plot of **CAN-2** is situated on the far left of Figure 4c, as very high temperatures were required to allow relaxation within a reasonable time frame. **CAN-1** and **CAN-3–9** showed relaxation in the same temperature range, however, the Arrhenius plot of **CAN-1** was shifted to significantly longer relaxation times at a certain temperature compared to the phenylpropynone-derived materials. Similar activation energies in the range of 124–137 kJ mol^{-1} were observed for **CAN-1,3,4,7–9**, whereas higher activation energies in the range of 179–198 kJ mol^{-1} were observed for **CAN-2,5,6**. This difference is expected to originate from the presence of electronically deactivating groups (ester functionality in **CAN-2** or electron donating *para*-substituents in **CAN-5,6**). Figure 4d displays an overview of stress relaxation curves at 130 °C of the networks to visualize the difference in relaxation times. Besides **CAN-2** which did not show relaxation at 130 °C, **CAN-1** showed the slowest relaxation at 130 °C (5030 s), whereas the fastest relaxation was observed for **CAN-7** (64 s).

The trends in exchange rate for different alkynone cross-linkers, as determined from kinetic model studies and DFT calculations, were not exactly reproduced on material level (Figure 4e). Moreover, the difference in stress relaxation times between phenylpropynone-derived materials (**CAN-3–9**) was not as pronounced as could be anticipated based on the remarkable differences in chemical relaxation times (Figure 1d). Nevertheless, compared to the unsubstituted reference (**CAN-3**), electron-withdrawing *para*-substituents still showed faster relaxation (**CAN-7,8,9**), whereas electron donating *para*-substituents exhibited slower relaxation (**CAN-5,6**), conserving the overall trends. Only **CAN-4** did not follow this trend and showed a faster relaxation than the unsubstituted reference (**CAN-3**), but this effect can be attributed to an increased mobility in the matrix as also shown during DSC analysis ($T_{g,\text{CAN-3}} > T_{g,\text{CAN-4}}$). Similarly, the difference in T_g could also explain the discrepancy in the ranking of **CAN-7,8,9**, where the high T_g of **CAN-9** indicates a restricted mobility, resulting in a slower relaxation time compared to **CAN-7,8**. These observations highlighted again the fact that exchange on a material level is not only controlled by the kinetics of dynamic bond exchange, but will also be substantially influenced by matrix effects, that are not captured by small molecule models.[3]

It is important to note that in the absence of an associative bond exchange mechanism, the prepared CANs cannot be classified as vitrimers, despite the observed linear relationship of relaxation times and temperature in the Arrhenius plots (Figure 4c). To illustrate the dissociative bond exchange mechanism operating in dynamic thiol–yne networks, frequency sweep measurements were performed at different temperatures. Whereas associative CANs or vitrimers are characterized by a constant plateau modulus G' at different temperatures as a result of their overall constant and temperature-independent cross-link density, dissociative CANs should show a decreasing G' with increasing temperature as a result of a net de-cross-linking.[5,52] Figure 5 shows the frequency sweep measurements for **CAN-1** and **CAN-3** as representative networks. As expected, a temperature-dependent decreasing plateau modulus was observed, confirming well the dissociative nature of the dynamic bond exchange. It is clear that despite this de-cross-linking, none of the CANs, with exception of **CAN-6** (Supporting Information, Figure S10), go through a gel-to-sol transition within the probed temperature range, and there is thus no sudden drop in viscosity in the stress relaxation experiments.

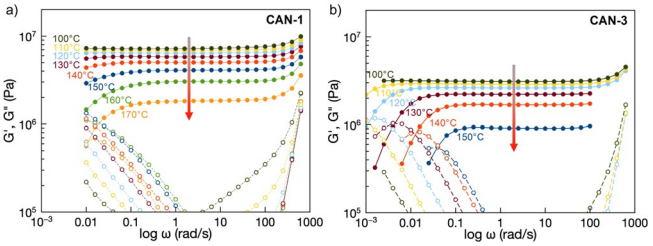

Figure 5. Frequency sweep measurements of a) **CAN-1** and b) **CAN-3**. Full circles: G', empty circles: G''.

Our small molecule models showed fast bond exchanges already happening at room temperature for most alkynones. On the other hand, the macroscopic exchange kinetics in the thiol–yne networks was much slower, with a much more pronounced temperature dependence (that is, activation energy). To study the network integrity of the prepared CANs at lower to ambient temperatures, creep experiments are most suitable. These were performed on **CAN-1** and **CAN-3** as representative networks (Supporting Information, Figure S15a,b). Both networks showed full shape recovery after deformations at 60 and 80 °C. However, a permanent deformation of both materials became prominent at temperatures above 100 °C, indicating activation of the dynamic chemistry. In line with previous observations in the stress relaxation experiments, the creep resistance of **CAN-1** was better than the one of **CAN-3** as a result of slower exchange. Also here, the relation between the creep rate ($\dot{\varepsilon}$) and temperature (T) was fitted to the Arrhenius equation to retrieve the corresponding activation energy (E_a) from the slope of the linear fit (Supporting Information, Figure S16).[15] The determined E_a was similar for both CANs, but about 30 kJ mol^{-1} lower than the E_a obtained during stress relaxation experiments.

Reprocessability of CANs

Following the study on the viscoelastic properties of the dynamic networks, the mechanical properties of these materials upon reprocessing were analyzed. For this purpose, **CAN-1** and **CAN-3** were subjected to 5 cutting/reprocessing cycles using

thermal compression molding at 140 °C for 30 minutes while monitoring their properties. Figure 6a,c shows the stress–strain curves of the original materials and after each reprocessing step. Since **CAN-1** has a T_g below room temperature, the material showed low stress and high strain, in contrast to **CAN-3**, with a T_g above room temperature. Upon reprocessing, the elongation, stress at break, and Young modulus remained very similar for **CAN-1**, proving adequate restoration of the original properties (Figure 6b). For **CAN-3**, a slight increase of the elongation and stress at break was observed (Figure 6d). The reprocessed materials also showed similar properties when monitored using swelling experiments (Supporting Information, Table S1), DSC analysis (Supporting Information, Figure S17), Fourier transform IR spectroscopy (Supporting Information, Figure S18), and Raman spectroscopy (Supporting Information, Figure S19). Although the restoration of the original properties was successful in these recycling experiments, it was observed that **CAN-1** required slightly longer remolding times after the third reprocessing cycle to regenerate a sample with the same properties, which implied some type of ageing. In an attempt to accelerate and exaggerate thermal ageing effects upon reprocessing, consecutive stress relaxation measurements were performed at 170 °C on **CAN-1** and **CAN-3** (Supporting Information, Figures S20, S21). Even though full relaxation was attained for both networks, an increased modulus upon each reprocessing cycle was observed, which was accompanied with an increased relaxation time. This effect can be readily rationalized by two factors, the first one being catalyst ageing (thermal degradation) leading to slower/less bond exchanges. Another explanation is that the networks become more perfect after reprocessing, as the virgin materials were found to still contain significant amounts of uncured VTE functions (ca. 10%; see above).

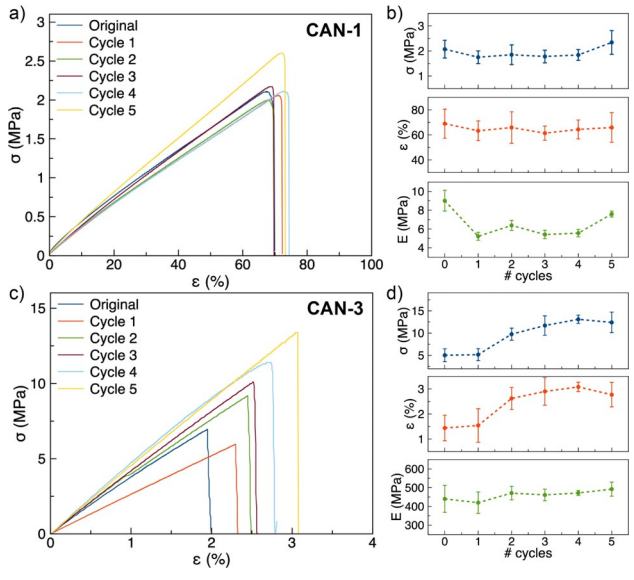

Figure 6. Overview of tensile strength experiments. a) Representative stress-strain curves of reprocessed **CAN-1**. b) Young modulus (E), strain (ε), and stress values (σ) after each reprocessing cycle of **CAN-1**. c) Representative stress–strain curves of reprocessed **CAN-3**. d) Young modulus, strain and stress values after each reprocessing cycle of **CAN-3**.

Conclusion

This work demonstrates the use of simple activated alkyne species as versatile dynamic cross-linkers for thiol–yne based polymer networks, resulting in a promising new chemical platform for the design of covalent adaptable networks. A wide series of alkynone precursors was explored for their click-like cross-linking reactivity that can join two thiols into a dynamic thioacetal linkage. Kinetic model studies revealed that exchange rates were significantly influenced by the steric and electronic nature of the alkyne cross-linker, with exchange rate constants spanning several orders of magnitude. Diverse substituents on a phenylpropynone scaffold showed a clear trend in rate effects, showing faster exchange rates for electron withdrawing substituents, and slower rates for electron donating groups. This behavior is in line with mechanistic expectations and was also further rationalized by density functional theory calculations.

The dynamic thiol–yne platform was subsequently implemented in materials to produce CANs. An extensive rheological analysis was performed to probe the interdependence of chemical structure and the dynamic network properties. A remarkable difference was observed in macroscopic network relaxation times, compared to the chemical exchange rates observed in small molecule models. Whereas the chemical exchange is already quite dynamic at or just above room temperature in small molecule models, the corresponding thiol–yne networks proved to be much less reactive, also confirmed by creep experiments. This demonstrates that overreliance on chemical model reactions for the design of CANs may be a misleading approach. Indeed, the thermodynamic landscape of bond exchange pathways can be quite dramatically altered by the macromolecular matrix and context.

The prepared dynamic networks showed excellent reprocessability and overall network integrity as proven by mechanical and thermal characterization, showing that this new chemistry platform could be further explored in many application areas for which CANs are being investigated. Not only can this reversible chemistry be used for reversible cross-linking in the context of CANs, but also in other dynamic applications and concepts, such as reversible functionalization, reversible polymerization, dynamic combinatorial libraries, etc. Especially the double functionality of the activated yne can lead to interesting dynamic applications and new concepts. In conclusion, this platform opens up many new avenues for further research within the field of CANs.

Acknowledgements

N.V.H. and M.G. acknowledge the Research Foundation—Flanders (Fonds Wetenschappelijk Onderzoek—Vlaanderen) for Ph.D. and Postdoctoral fellowships. K.U. acknowledges UGent for funding. F.E.D.P acknowledges UGent funding (BOF-GOA). B. De Meyer, J. Goeman, and T. Courtin are thanked for technical support. The computational resources (Stevin Supercomputer Infrastructure) and services used in this work were provided by the VSC (Flemish Supercomputer Center), funded by Ghent University, FWO and the Flemish Government—department EWI.

Conflict of interest

The authors declare no conflict of interest.

Keywords: covalent adaptable networks · cross-linking · Michael addition · thioacetals · thiol–yne

How to cite: *Angew. Chem. Int. Ed.* **2020**, *59*, 3609 – 3617
Angew. Chem. **2020**, *132*, 3637 – 3646

[1] C. J. Kloxin, C. N. Bowman, *Chem. Soc. Rev.* **2013**, *42*, 7161 – 7173.
[2] G. M. Scheutz, J. J. Lessard, M. B. Sims, B. S. Sumerlin, *J. Am. Chem. Soc.* **2019**, https://doi.org/10.1021/jacs.9b07922.
[3] J. Winne, L. Leibler, F. E. Du Prez, *Polym. Chem.* **2019**, Accepted.
[4] M. K. McBride, B. T. Worrell, T. Brown, L. M. Cox, N. Sowan, C. Wang, M. Podgorski, A. M. Martinez, C. N. Bowman, *Annu. Rev. Chem. Biomol. Eng.* **2019**, *10*, 175 – 198.
[5] P. Chakma, D. Konkolewicz, *Angew. Chem. Int. Ed.* **2019**, *58*, 9682 – 9695; *Angew. Chem.* **2019**, *131*, 9784 – 9797.
[6] W. Denissen, J. M. Winne, F. E. Du Prez, *Chem. Sci.* **2016**, *7*, 30 – 38.
[7] X. Chen, M. A. Dam, K. Ono, A. Mal, H. Shen, S. R. Nutt, K. Sheran, F. Wudl, *Science* **2002**, *295*, 1698 – 1702.
[8] Y. Higaki, H. Otsuka, A. Takahara, *Macromolecules* **2006**, *39*, 2121 – 2125.
[9] S. Billiet, K. De Bruycker, F. Driessen, H. Goossens, V. Van Speybroeck, J. M. Winne, F. E. Du Prez, *Nat. Chem.* **2014**, *6*, 815 – 821.
[10] H. A. Houck, K. De Bruycker, C. Barner-Kowollik, J. M. Winne, F. E. Du Prez, *Macromolecules* **2018**, *51*, 3156 – 3164.
[11] N. Van Herck, F. E. Du Prez, *Macromolecules* **2018**, *51*, 3405 – 3414.
[12] M. Delahaye, J. M. Winne, F. E. Du Prez, *J. Am. Chem. Soc.* **2019**, *141*, 15277 – 15287.
[13] D. Montarnal, M. Capelot, F. Tournilhac, L. Leibler, *Science* **2011**, *334*, 965 – 968.
[14] W. Denissen, G. Rivero, R. Nicolaÿ, L. Leibler, J. M. Winne, F. E. Du Prez, *Adv. Funct. Mater.* **2015**, *25*, 2451 – 2457.
[15] M. Guerre, C. Taplan, R. Nicolaÿ, J. M. Winne, F. E. Du Prez, *J. Am. Chem. Soc.* **2018**, *140*, 13272 – 13284.
[16] Y. Spiesschaert, M. Guerre, L. Imbernon, J. M. Winne, F. Du Prez, *Polymer* **2019**, *172*, 239 – 246.
[17] C. Taplan, M. Guerre, J. M. Winne, F. E. Du Prez, *Mater. Horiz.* **2019**, https://doi.org/10.1039/C9MH01062A.
[18] B. Hendriks, J. Waelkens, J. M. Winne, F. E. Du Prez, *ACS Macro Lett.* **2017**, *6*, 930 – 934.
[19] M. M. Obadia, A. Jourdain, P. Cassagnau, D. Montarnal, E. Drockenmuller, *Adv. Funct. Mater.* **2017**, *27*, 1703258.
[20] T. F. Scott, A. D. Schneider, W. D. Cook, C. N. Bowman, *Science* **2005**, *308*, 1615 – 1617.
[21] W. A. Ogden, Z. Guan, *J. Am. Chem. Soc.* **2018**, *140*, 6217 – 6220.
[22] B. Zhang, Z. A. Digby, J. A. Flum, P. Chakma, J. M. Saul, J. L. Sparks, D. Konkolewicz, *Macromolecules* **2016**, *49*, 6871 – 6878.
[23] J. S. A. Ishibashi, J. A. Kalow, *ACS Macro Lett.* **2018**, *7*, 482 – 486.
[24] G. Joshi, E. V. Anslyn, *Org. Lett.* **2012**, *14*, 4714 – 4717.
[25] B. M. Matysiak, P. Nowak, I. Cvrtila, C. G. Pappas, B. Liu, D. Komaromy, S. Otto, *J. Am. Chem. Soc.* **2017**, *139*, 6744 – 6751.
[26] P. Chakma, L. H. Rodrigues Possarle, Z. A. Digby, B. Zhang, J. L. Sparks, D. Konkolewicz, *Polym. Chem.* **2017**, *8*, 6534 – 6543.
[27] S. P. Daymon, K. M. Miller, *Polymer* **2018**, *145*, 286 – 293.
[28] N. Kuhl, R. Geitner, R. K. Bose, S. Bode, B. Dietzek, M. Schmitt, J. Popp, S. J. Garcia, S. van der Zwaag, U. S. Schubert, et al., *Macromol. Chem. Phys.* **2016**, *217*, 2541 – 2550.
[29] B. T. Worrell, S. Mavila, C. Wang, T. M. Kontour, C.-H. Lim, M. K. McBride, C. B. Musgrave, R. Shoemaker, C. N. Bowman, *Polym. Chem.* **2018**, *9*, 4523 – 4534.
[30] S.-H. Shim, M. Ham, J. Huh, Y.-K. Kwon, Y.-J. Kwark, *Polym. Chem.* **2013**, *4*, 5449.
[31] L. J. Macdougall, V. X. Truong, A. P. Dove, *ACS Macro Lett.* **2017**, *6*, 93 – 97.
[32] A. B. Lowe, *Polymer* **2014**, *55*, 5517 – 5549.
[33] D. P. Nair, M. Podgórski, S. Chatani, T. Gong, W. Xi, C. R. Fenoli, C. N. Bowman, *Chem. Mater.* **2014**, *26*, 724 – 744.
[34] H. Kuroda, I. Tomita, T. Endo, *Polymer* **1997**, *38*, 6049 – 6054.
[35] O. Daglar, U. S. Gunay, G. Hizal, U. Tunca, H. Durmaz, *Macromolecules* **2019**, *52*, 3558 – 3572.
[36] C. Xu, J. K. Bartley, D. I. Enache, D. W. Knight, M. Lunn, M. Lok, G. J. Hutchings, *Tetrahedron Lett.* **2008**, *49*, 2454 – 2456.
[37] M. Zheng, F. Wu, K. Chen, S. Zhu, *Org. Lett.* **2016**, *18*, 3554 – 3557.
[38] G. Ieronimo, G. Palmisano, A. Maspero, A. Marzorati, L. Scapinello, N. Masciocchi, G. Cravotto, A. Barge, M. Simonetti, K. L. Ameta, et al., *Org. Biomol. Chem.* **2018**, *16*, 6853 – 6859.
[39] J. M. Wilbur, B. A. Bonner, *J. Polym. Sci. Part A* **1990**, *28*, 3747 – 3759.
[40] V. X. Truong, A. P. Dove, *Angew. Chem. Int. Ed.* **2013**, *52*, 4132 – 4136; *Angew. Chem.* **2013**, *125*, 4226 – 4230.
[41] D.-J. Zhang, M.-S. Xie, G.-R. Qu, Y.-W. Gao, H.-M. Guo, *Org. Lett.* **2016**, *18*, 820 – 823.
[42] Y. S. Lee, K. H. Chung, Y. H. Kim, *Heteroat. Chem.* **1999**, *10*, 461 – 464.
[43] Y. Zhong, Y. Xu, E. V. Anslyn, *Eur. J. Org. Chem.* **2013**, 5017 – 5021.
[44] B. Zhang, P. Chakma, M. P. Shulman, J. Ke, Z. A. Digby, D. Konkolewicz, *Org. Biomol. Chem.* **2018**, *16*, 2725 – 2734.
[45] E. H. Krenske, R. C. Petter, K. N. Houk, *J. Org. Chem.* **2016**, *81*, 11726 – 11733.
[46] M. Capelot, M. M. Unterlass, F. Tournilhac, L. Leibler, *ACS Macro Lett.* **2012**, *1*, 789 – 792.
[47] J. Van Damme, O. van den Berg, J. Brancart, L. Vlaminck, C. Huyck, G. Van Assche, B. Van Mele, F. Du Prez, *Macromolecules* **2017**, *50*, 1930 – 1938.
[48] P. J. Flory, *J. Am. Chem. Soc.* **1941**, *63*, 3083 – 3090.
[49] W. H. Stockmayer, *J. Chem. Phys.* **1943**, *11*, 45 – 55.
[50] L. H. Sperling, *Introduction to Physical Polymer Science*, Wiley, Hoboken, **2005**.
[51] C. Jehanno, I. Flores, A. P. Dove, A. J. Müller, F. Ruipérez, H. Sardon, *Green Chem.* **2018**, *20*, 1205 – 1212.
[52] P. J. Flory, *Chem. Rev.* **1944**, *35*, 51 – 75.

Manuscript received: October 9, 2019
Revised manuscript received: November 22, 2019
Accepted manuscript online: December 17, 2019
Version of record online: January 23, 2020

